Beyond PCBM: Understanding the Photovoltaic Performance of Blends of Indene-C_{60} Multiadducts with Poly(3-hexylthiophene)

*Alexandre M. Nardes, Andrew J. Ferguson, James B. Whitaker, Bryon W. Larson, Ross E. Larsen, Klára Maturová, Peter A. Graf, Olga V. Boltalina, Steven H. Strauss, and Nikos Kopidakis**

The effect of functionalization of the C_{60} cage with multiple indene groups in relation to the dynamics of photogenerated species in blends with poly(3-hexylthiophene) (P3HT) and the performance of P3HT:indene-C_{60} photovoltaic devices is reported. Despite the systematic decrease of the electron affinity of the acceptor with the number of additions, exciton dissociation is efficient in blends of P3HT with all three indene-C_{60} derivatives. By replacing the prototypical acceptor [6,6]-phenyl-C_{61}-butyric acid methyl ester (PCBM) with mono-indene-C_{60} (ICMA) or a sample of a mixture of bis-indene-C_{60} regioisomers (ICBA) the power conversion efficiency is enhanced, predominantly due to an increase in the open-circuit voltage that originates from the lower electron affinity of the indene-C_{60} acceptor. The use of an acceptor sample that represents a mixture of tris-indene-C_{60} (ICTA) regioisomers results in a reduction of the short-circuit current density, fill factor, and open-circuit voltage of the photovoltaic device. The electron mobility in ICTA domains is ca. a factor 10 lower than in ICMA and ICBA. Density functional theory calculations of the LUMO energies in ICTA isomers demonstrate that energetic disorder caused by the presence of regioisomers is unlikely to be responsible for the low electron mobility in ICTA. The observed deterioration in device performance is attributed to the formation of small ICTA clusters "coated" in insulating indene units that reduce electronic coupling between the molecules and cause the low electron mobility in ICTA domains. These findings indicate that while multiple additions to a fullerene cage provide a facile methodology for controlling the energy levels, they may have limited success in improving OPV device performance.

1. Introduction

The confirmed power conversion efficiency (PCE) of solution-processed organic photovoltaics (OPV) with donor-acceptor (D-A) bulk-heterojunction (BHJ) active layers has increased from 3.0 to 8.3% over the past 4 years.[1] This remarkable progress is in large part due to the tunability afforded in organic materials by seemingly simple modifications of their molecular structure, that led to the development of donor and acceptor materials with improved properties for solar energy conversion. Design rules for new materials to push toward PCEs of 10% were formulated by Scharber et al. in 2006,[2] which have led to two main areas of materials development: a) lowering the absorption onset of the conjugated polymer light-harvesting component, thereby improving overlap with the solar spectrum, to increase the short circuit current, J_{sc}[3] and b) tuning the relative energetics of the ionization potential of the donor (IP_D) and the electron affinity of the acceptor (EA_A) to improve the open-circuit voltage, V_{oc}.[3a,3b,3e,3g,4] This paper pertains to the latter mechanism; we investigate a class of fullerene-based molecular acceptors that, when used in BHJ OPV devices, improve the V_{oc} as compared to the prototypical acceptor PCBM,[4i,4m] and study the photoinduced dynamics of excitons and free carriers as a function of the chemical structure of the molecular acceptor, which is directly related to EA_A.

Although increased V_{oc}, and in some instances enhanced PCE, have been demonstrated in polymer:fullerene OPV devices with acceptors with lower EA_A,[4] in the case of the multiadducts of [6,6]-phenyl-C_{61}-butyric acid methyl ester (PCBM) an undesirable reduction in photocurrent has been observed,[4f,4g] which has been attributed to a reduction in the electron mobility with increasing number of solubilizing side chains, particularly in the case of the tris-adduct. It is plausible that modification of

Dr. A. M. Nardes, Dr. A. J. Ferguson, Dr. R. E. Larsen, Dr. K. Maturová, Dr. P. A. Graf, Dr. N. Kopidakis
National Renewable Energy Laboratory
1617 Cole Blvd, Golden, CO 80401, USA
E-mail: nikos.kopidakis@nrel.gov
J. B. Whitaker, B. W. Larson, Dr. O. V. Boltalina, Prof. S. H. Strauss
Department of Chemistry
Colorado State University
Fort Collins, CO 80523, USA

DOI: 10.1002/adfm.201200336

the fullerene can influence i) charge transport, particularly in the fullerene domain,[4f,4g] either due to energetic disorder[5] or changes in the microstructure of the blend,[4g] and ii) the efficiency of charge generation.[6]

It has been reported that the efficiency of photoinduced electron transfer is close to unity for the BHJ system based on the conjugated polymer poly(3-hexylthiophene) (P3HT) and PCBM,[7] indicating that P3HT is a suitable polymer with which to probe photoinduced processes as a function of molecular structure of the fullerene-based acceptor. In this paper we study the dynamics of exciton dissociation and free carrier generation and decay in blends of P3HT with three commercially available C_{60}-based acceptors. These are mono-indene-C_{60}, (ICMA) and the higher adducts bis- (ICBA) and tris-indene-C_{60}, (ICTA),[8] which have been used previously in OPV devices where a higher open-circuit voltage was attributed to the lower EA_A of the acceptors than that of PCBM.[4i,4m] Here we rationalize the observed device performance and photophysical properties by chemical characterization of the samples and density functional theory calculations of the LUMO energies of the isomers of three indene-C_{60} derivatives. The scope of this paper is to understand how the extent of fullerene cage substitution affects the electronic, photophysical and carrier transport properties in blends of indene-C_{60} derivatives with the prototypical conjugated polymer P3HT. We show that the as-received indene-C_{60} multiadduct samples are likely to include small amounts of lower and/or higher adducts, in addition to the expected distribution of isomers in the case of ICBA and ICTA, which would all be expected to strongly influence the photophysical and optical properties. Their cyclic voltammograms in solution demonstrate negative shifts of the $E_{1/2}$ values relative to PCBM of 0.12, 0.16, and 0.36 V for ICMA, ICBA and ICTA, respectively, that corresponds to lower EA_A in the indene-C_{60} derivatives compared to PCBM and a gradual lowering of EA_A from the mono-, bis- and tris-adducts, as reported previously.[4m,8] We use the time-correlated single photon counting (TCSPC) and the contactless flash-photolysis time-resolved microwave conductivity (FP-TRMC) spectroscopic techniques to probe the exciton lifetime, and the generation and decay of free electrons and holes, in films of P3HT blended with the indene-C_{60} derivatives. We show that the efficiency of exciton quenching decreases slightly as EA_A decreases and that the observed quenching results in the efficient formation of free carriers. We show that this decrease is not sufficient to account for the observed poor PV device performance when the ICTA acceptor is used. We find that the high-frequency electron mobilities measured by TRMC in ICMA and ICBA blended with P3HT are comparable to that measured in PCBM,[9] but that the mobility decreases by a factor of 10 in ICTA. Analysis of the photoconductance transients confirms the low mobility in the ICTA domains. DFT calculations show that the energies of the LUMO vary by ca. 50 meV among isomers of both ICBA and ICTA, which is not enough to account for the severe drop in the mobility in ICTA. We suggest that the very presence of the three bulky indene groups results in the formation of small ICTA clusters that position the insulating indene units on the outside, thus reducing both the local (high-frequency) mobility and, correspondingly, the bulk transport of electrons between fullerene clusters. In addition, the third indene unit may push the C_{60} cages further apart, resulting in decreased electronic coupling between ICTA molecules, as recently proposed.[10]

2. Results and Discussion

2.1. Chemical Characterization of the Indene-C_{60} Samples

The compositional and isomeric purity of an acceptor compound may affect its performance in an OPV device when the impurities or different isomers of an acceptor have significantly different electronic properties, molecular structures or solubilities. For example, it has been shown that the introduction of a few percent of $PC_{84}BM$ impurity, with higher EA_A, in the $PC_{60}BM$ acceptor results in deterioration of the OPV device performance due to trap-limited electron transport.[11] The reported syntheses of ICMA, in a Diels-Alder [4 + 2] cycloaddition reaction of C_{60} with isoindene have been shown to produce a single [6,6]-adduct in 25-35% yield, and its isolation by flash chromatography can result in high purity samples as evidenced by nuclear magnetic resonance (NMR) spectroscopy.[4i,4m,12] Formation of multiadducts, i.e., ICBA and ICTA, was found to be favored when longer reaction times and higher equivalents of isoindene were applied; the highest reported yield of 54% for ICBA, which was found to comprise a mixture of isomers as evidenced by high-performance liquid chromatography (HPLC) and NMR spectroscopy, was achieved in a continuous flow reactor.[13] In an earlier study, the purified ICBA sample was proposed to consist of a single trans isomer at 97% purity,[4i] but this claim was subsequently corrected to state that ICBA was a mixture of six isomers.[14] To our knowledge, there have not been reports on the isolation of the pure isomers of ICBA or ICTA. These reports prompted us to perform analysis of the commercial indene-C_{60} samples used in this work by means of HPLC, NMR spectroscopy and mass spectrometry.

2.1.1. HPLC Analysis

Figure 1 shows HPLC traces for ICMA, ICBA and ICTA samples recorded on a Cosmosil Buckyprep column commonly used for fullerene analysis and separation. Use of a relatively polar eluent (100% toluene) showed either broad single peaks (for ICMA and ICTA) or a poorly resolved two-peak band (ICBA), and all had short retention times of 4-5 minutes. In addition to the multipeak shape for ICBA, the shape of the traces for ICMA and ICTA indicated that they probably contain multiple components. Therefore, when a series of less polar eluents were applied for analysis, a more efficient separation was achieved, revealing that all three samples had multiple components. We note here that only a rough estimation of the lower limit of the number of components can be made due to limitations of the method (see more on HPLC analysis in SI). The insets in Figure 1 show HPLC traces in 30/70 v/v toluene/heptane mixture for all three samples. Importantly, the ranges of their retention times, t_R, can now be differentiated, with the longest retention being exhibited by ICMA (t_R = 14-22 min), followed by ICBA (t_R = 11-17 min) and ICTA (t_R = 9-14 min). Such order of elution is typical for multiadducts of fullerenes, and it can be tentatively correlated

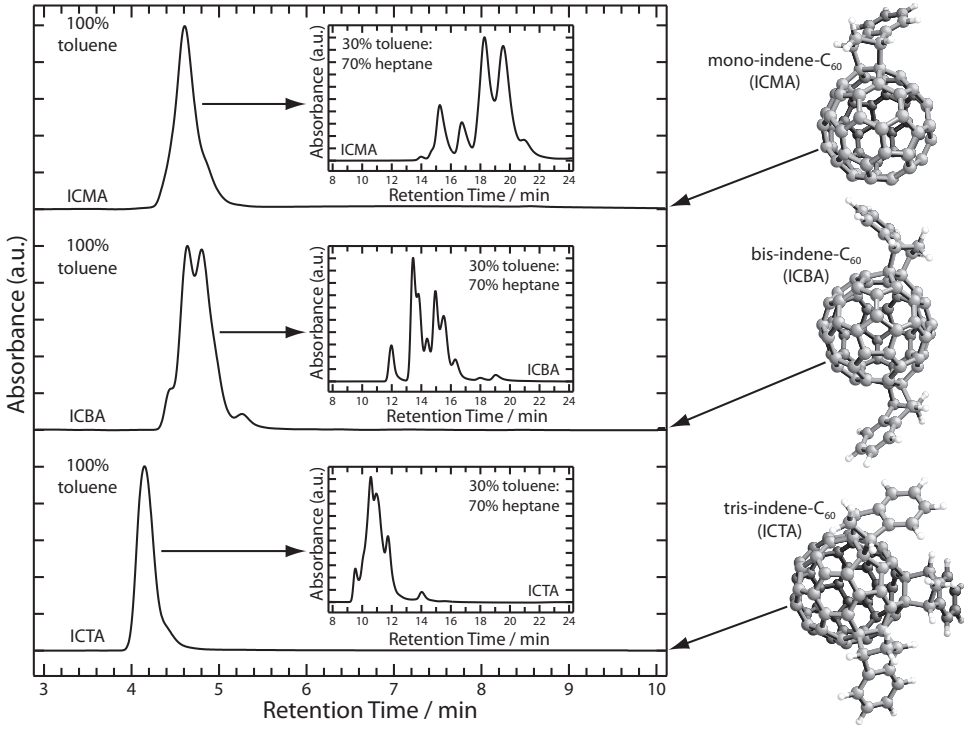

Figure 1. HPLC traces of ICMA, ICBA, and ICTA (top to bottom, respectively) in 100% toluene eluent using a Cosmosil Buckyprep column with 20 mm i.d. × 250 mm dimensions and a flow rate of 16 mL min^{-1}. Insets: HPLC traces of the corresponding sample in a 30/70 v/v eluent mixture of toluene/heptane. The detection wavelength was 300 nm. The DFT-optimized molecular structures of representative isomers of ICMA, ICBA and ICTA are also shown.

with the relative polarities of the indene adducts and the size of the remaining π-system of the fullerene cage that is primarily responsible for interaction with the stationary phase of the column. There is a partial overlap in the elution bands between the three samples that may be due either to cross-contamination (e.g., presence of ICBA isomers in ICMA sample, and so on) originating from the imperfect separation of the crude reaction product or simply to the different isomers of multiadducts possessing similar retention properties (e.g., some isomers of ICTA may have the same retention times as some isomers of ICBA). We therefore cannot rule out the presence of some ICBA isomers in the ICMA and ICTA samples, or ICMA and/or ICTA isomers in the ICBA sample by this analysis alone.

2.1.2. Mass Spectrometry Analysis

To further explore the possibility of cross-contamination between the different multiadducts we first applied atmospheric pressure chemical ionization (APCI) mass spectrometry, which has previously been demonstrated as applicable for the analysis of many thermally labile soluble fullerene derivatives.[15] Molecular ions of ICMA (m/z 836), ICBA (m/z 953) and ICTA (m/z 1069) were indeed observed in the respective samples in the negative mode, and their assignment was confirmed by collision-induced dissociation experiments and correct isotope distribution (see Supporting Information for APCI mass spectra). However, the intensities of molecular anion peaks for the indene-C_{60} multiadducts were low due to reduced EA_A values compared to C_{60} and because of partial fragmentation (consecutive loss of multiple indene moieties) under mass spectrometry conditions. While the latter prevents an unambiguous determination of the molecular compositions of ICBA and ICTA samples with respect to the presence of lower adducts, we were able to determine that significant amounts of ICBA isomers were present in the ICMA sample, in agreement with the HPLC data. In an attempt to resolve this issue the multiadduct samples were analyzed by matrix-assisted laser-desorption-ionization time-of-flight (MALDI-TOF) mass spectrometry, but similar partial fragmentation was also observed in the mass spectra, in agreement with the recently published MALDI-TOF mass spectrometry data for ICBA and ICTA.[4m]

2.1.3. NMR Analysis

The ^{1}H NMR spectra were recorded for all three samples and compared to the available literature data. Notably, the ICMA sample exhibited a more complex spectrum than expected for a single [6,6] mono-adduct, indicating that the purity of ICMA sample is lower than 50%, while the other components are most likely isomers of ICBA, in accordance with the APCI mass spectrometry data. The ^{1}H NMR spectrum of the ICBA sample consists of many poorly resolved multiplets, but its general features are very similar to those reported in the literature.[13] The ^{1}H NMR spectrum of ICTA sample is even more complex and poorly resolved which agrees with the presence of multiple isomers of multiadducts (see Supporting Information).

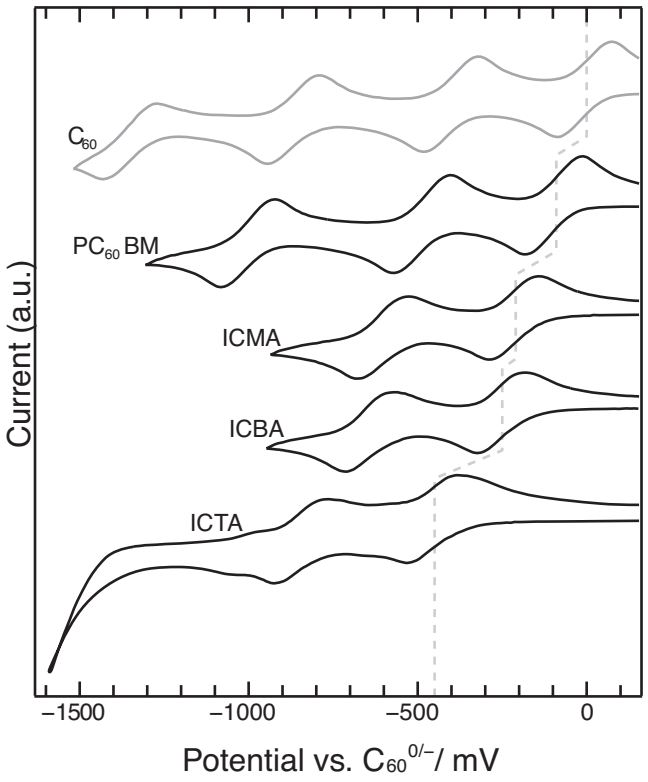

Figure 2. The impact of indene-substitution on the position of the reduction potential of the fullerene derivatives measured using cyclic voltammetry vs. C_{60} for PCBM, ICMA, ICBA and ICTA. The first reduction of C_{60} is placed at 0 mV on the abscissa. The dashed line indicates the shift in the first half-wave reduction potential upon fullerene substitution.

2.1.4. Cyclic Voltammetry

To elucidate the impact of the inadvertent contaminants on EA_A cyclic voltammograms were measured to determine the reduction potentials in *ortho*-dichlorobenzene (**Figure 2**). These demonstrate cathodic shifts of the $E_{1/2}$ reduction values relative to PCBM of 0.12, 0.16, and 0.36 V for ICMA, ICBA and ICTA, respectively, (**Table 1**) that corresponds to a reduced EA_A in the indene-C_{60} derivatives compared to PCBM. We note that the CV of these complex mixtures shows quasi-reversible first and second reductions (for a scan speed of 20 mV s^{-1}) for all three samples and that only ICTA exhibits significant broadening of the first reduction peak (as well as the presence of small shoulders between the main peaks), which may be indicative of the presence of several components with slightly varying redox properties. The $E_{1/2}$ value for ICMA measured in this work shows a larger difference with that measured for PCBM and a smaller difference with that measured for ICBA than reported in the literature,[4i,4m] which is most likely due to the presence of ICBA isomers in our ICMA sample.

In summary, the HPLC and mass-spectroscopic characterization of the three indene-C_{60} adduct samples used in this work revealed that none of the samples represented a pure single isomer derivative. At least ten different components are present in ICTA, whereas seven or more components are found in the ICBA sample. Notably, we observe that the ICMA sample is considerably contaminated with bis-adducts. The precise nature of the molecular compositions is currently difficult to evaluate due to the observed fragmentation in the mass spectra, highlighting the need to develop a mass spectrometry technique with softer ionization than the MALDI or APCI used in this study. Although the CV data are suggestive of the presence of ICBA impurities in the ICMA sample and the presence of several components in the ICTA sample, the technique is not sufficiently sensitive to clearly resolve the redox properties of the individual isomers. We therefore calculated LUMO energies of isomers of indene multiadducts by DFT, and the results are discussed in the next section.

Table 1. Electrochemical characterization of the fullerene derivatives and photovoltaic characterization data for 1:1 P3HT:fullerene-based solar cell devices.

Acceptor	$E_{1/2,red1}$ [a)] [V vs. $C_{60}^{0/-}$]	V_{oc} [b)] [V]	I_{sc} [c)] [mA cm^{-2}]	FF [d)] [%]	PCE [e)] [%]	R_{series} [f)] [Ω]
PCBM	–0.09	0.56	11.05	56	3.40	19
ICMA	–0.21	0.69	10.56	54	3.92	112
ICBA	–0.25	0.78	10.82	56	4.65	105
ICTA	–0.45	0.69	1.86	40	0.51	454

[a)] $E_{1/2,red1}$ represents the first half-wave reduction potential (defined as the potential halfway between the anodic and cathodic peak potentials for the first reduction of the fullerene derivative) relative to $C_{60}^{0/-}$: For the P3HT:fullerene OPV devices; [b)] V_{oc} represents the open-circuit voltage; [c)] J_{sc} represents the short-circuit current density; [d)] FF represents the fill factor; [e)] PCE represents the power conversion efficiency; and [f)] R_{series} represents the series resistance.

2.2. DFT Calculations of the LUMO Energies

The addition of multiple substituents to the fullerene cage results in the possibility of a number of regioisomers for the ICBA and ICTA adducts, consistent with the chemical characterization data presented above, which gives rise to a distribution of lowest unoccupied molecular orbital (LUMO) energies. It has been suggested that the existence of multiple isomers can result in carrier trapping at sites occupied by fullerene adducts with lower LUMO energies,[5] which is detrimental to the electron mobility in fullerene domains. To evaluate the extent to which this energetic disorder within fullerene domains might play a role in electron transport we used density functional theory (DFT) to calculate the lowest unoccupied molecular orbital (LUMO) energies for the indene-C_{60} adducts (**Figure 3**a). DFT calculations show that an increase in the number of indene units attached to the fullerene cage pushes the LUMO closer to vacuum, consistent with the observed trend in the reduction potential measured by CV (Figure 2).

The different regioisomers of ICBA and ICTA were generated as described in the Experimental Section and DFT calculations were performed on the resulting structures with the Gaussian 09 electronic structure program.[16] Although steric restrictions were implemented to prevent neighboring indene units in the optimized geometry from being less than 1Å apart, the number of possible regioisomers was still 23 and 53 for ICBA and ICTA, respectively. The dashed lines in Figure 3b,c indicate

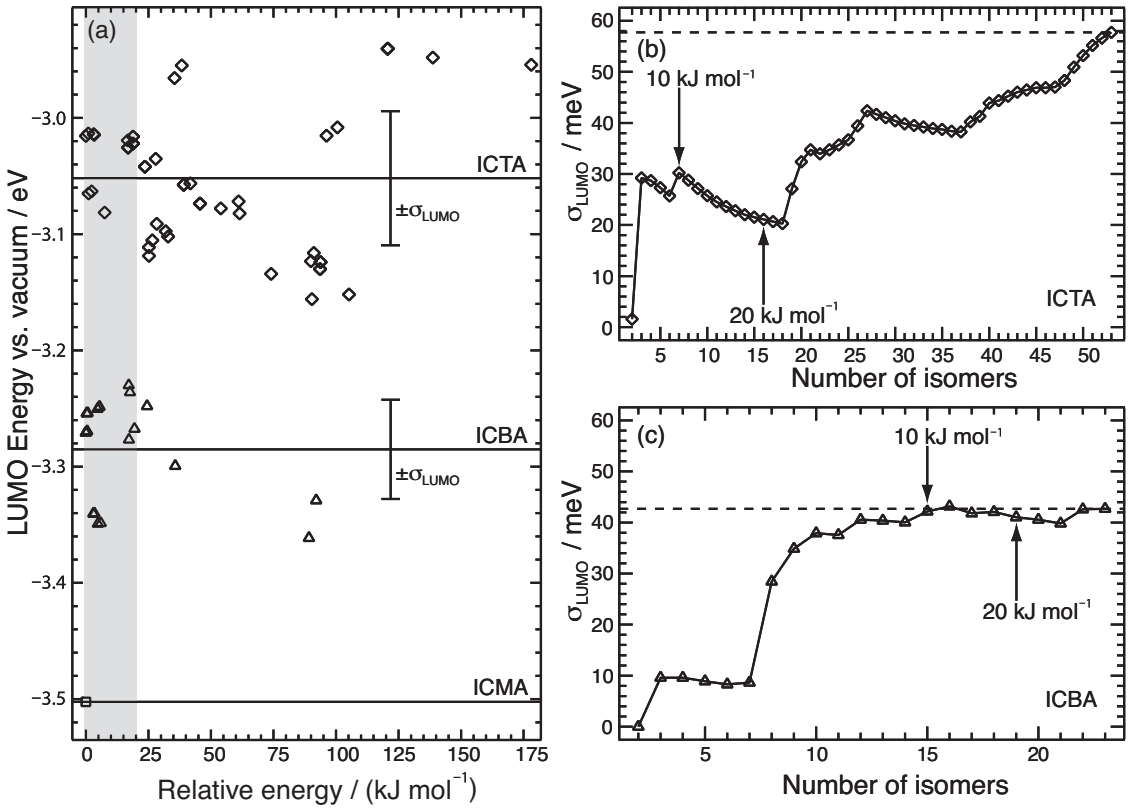

Figure 3. a) LUMO energies vs. the total isomer energy relative to the most stable isomer, calculated by DFT at the B3LYP/6-31G(d)//6-31+G(d) level, for ICMA (square), and isomers of ICBA (triangles) and ICTA (diamonds). The grey region encompasses the most stable ICBA and ICTA isomers (with relative energies <20 kJ mol^{-1}). For the ICBA and ICTA adducts the solid lines indicate the position of the mean LUMO energy and the vertical bars indicate one standard deviation from this mean. The standard deviation of the LUMO energy for b) ICBA and c) ICTA as a function of the number of isomers (N), calculated for the N lowest energy isomers. The arrows indicate the number of isomers within 10 and 20 kJ mol^{-1} of the most stable isomer, and the dashed lines indicate the standard deviation of the LUMO energy for all isomers considered in the DFT calculations.

the standard deviation of the LUMO energies for all isomers considered in DFT calculations, which would indicate that the spread in the LUMO energy is approximately 50% larger for the tris-adduct. In an analogous system the observed decrease in performance of P3HT:tris-PCBM devices, relative to those employing bis-PCBM as the electron acceptor,[4f] was originally attributed to an increase in the spread of the LUMO energies derived from differential pulse voltammetry and DFT calculations,[5] which results in trapping of electrons at fullerene sites possessing a deep-lying LUMO.

While the chemical characterization performed on the multi-adduct samples used in this study confirms the existence of multiple isomers, it also indicates that all possible isomers are not present, suggesting that only the LUMO energies of the most stable regioisomers should be considered. The grey region in Figure 3a highlights the isomers with relative energies <20 kJ mol^{-1} larger than the most stable isomer, and Figure 3b,c show the standard deviation of the LUMO energy as a function of the N lowest energy isomers for ICBA and ICTA, respectively. The arrows in Figure 3b,c indicate the presence of 19 regioisomers in the ICBA sample and 16 regioisomers in the ICTA sample that lie within 20 kJ mol^{-1} of the most stable isomer, in reasonable agreement with the HPLC data shown above. Importantly, this analysis shows that the spread (σ_{LUMO}) in the LUMO energies is actually smaller for ICTA than ICBA, for the most stable isomers. Since the electron mobility in the acceptor domains of P3HT:ICBA blends is slightly higher than that in P3HT:PCBM (vide infra), we conclude that energetic disorder of the magnitude observed here does not have a detrimental effect on electron transport (and, accordingly on the device performance also shown below) for active layers based on blends of P3HT with ICBA, and therefore also with ICTA, multiadducts.

2.3. P3HT:Fullerene BHJ Solar Cells

Bulk-heterojunction solar cells were fabricated using ICMA, ICBA and ICTA as acceptors. For comparison, devices were also made with the commonly used P3HT:PCBM blend. **Figure 4** shows *J–V* characteristics of all these OPV devices at room temperature under simulated AM1.5 illumination. The corresponding solar cell parameters are listed in Table 1.

A significant enhancement of the V_{oc} (90 mV) is observed for the device incorporating the bis-adduct (ICBA) compared to the mono-adduct (ICMA). Additionally, the results of devices employing PCBM, ICMA and ICBA as electron acceptors agree well with previous reports for the same systems,[4i] although a

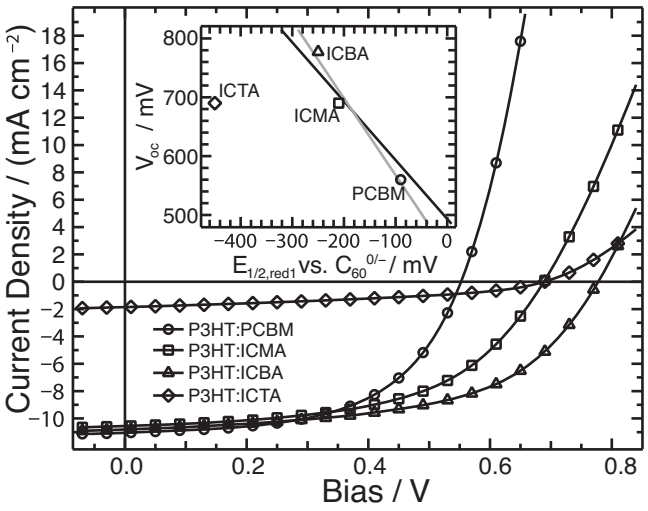

Figure 4. *J–V* characteristics of P3HT:fullerene BHJ solar cells. Active layers consist of P3HT blended in a 1:1 ratio by weight with PCBM (circles), ICMA (squares), ICBA (triangles), and ICTA (diamonds). The inset shows the measured V_{oc} as a function of the first half-wave reduction potential (relative to fullerene$^{0/-}$); the black line has a slope of –1, whereas the gray line is the best fit with a slope of –1.3.

larger increase in the V_{oc} of the P3HT:ICMA versus that with PCBM is observed here (130 mV) compared to previous work.[4i] The enhancement in the V_{oc} is summarized in the inset of Figure 4, the best fit to the V_{oc} vs $E_{1/2,red1}$ data for the devices with PCBM and ICMA and ICBA is a line with slope 1.3, which is close to the dependence observed previously in bulk heterojunctions with other fullerene derivatives.[17] As a result of the optimized V_{oc} the maximum PCE of 4.65% was achieved with the P3HT:ICBA device, although the use of an un-optimized Al cathode in this work (see below) means the PCE is lower than previously reported.[4i]

The enhanced V_{oc} for ICMA and ICBA is tempered by a small loss (ca. 5%) in J_{sc}, compared to the P3HT:PCBM device, which can be linked to the factor of five increase in the series resistance measured in the devices with ICMA and ICBA. We attribute this to the change in contact resistance at the interface between the Al cathode and the active layer. Measurements of P3HT:ICBA with optimized contacts (not shown), consisting of a Ca layer between the active layer and the Al electrode, used previously in similar devices,[4i] yield a reduced series resistance of ca. 50 Ω suggesting that the series resistance of our devices are limited by the contact and not the active layer in the ICMA and ICBA cases.

When ICTA is used as the acceptor material the J_{sc} decreases by nearly one order of magnitude, comparable to what has been observed when the tris-adduct of PCBM was used as an acceptor material in OPV devices.[4f,4g] A dramatic increase of the series resistance, to ca. 450 Ω, is also observed for the P3HT:ICTA device. As we will show below, this increase, compared to the values seen in the lower adducts, is mostly due to low electron mobility in the ICTA phase in the bulk-heterojunction. As a result of the very low J_{sc} and a severe series resistance limitation, the V_{oc} does not reach the value expected from the EA_A of this fullerene (the V_{oc} lies well below the trend line in the inset of Figure 4). We note that all the observed changes in performance (V_{oc}, J_{sc} and PCE) of the devices shown here agree qualitatively with previous results obtained for multiadducts of PCBM as electron acceptors.[4f,4g]

It should be noted that the likely presence of ICMA in the ICBA would result in the presence of very deep energetic traps that would be expected to drastically hinder the electron transport in the blend with the ICMA acceptor. This is obviously not the case, since the short circuit current in the P3HT:ICBA device is comparable to the devices employing PCBM and ICMA as the electron acceptor. This observation brings into question whether energetic trapping plays a role in the poor performance of the P3HT:ICTA device, since ICBA traps may also be present in addition to the distribution of LUMO energies due to the presence of multiple regioisomers.

2.4. Exciton Dissociation and Charge Carrier Generation

In this section we use TRMC and TCSPC on films of P3HT blended with indene-C_{60}-based acceptors to address the issues of exciton dissociation and charge carrier generation in these layers.

Typical photoconductance transients measured by TRMC after excitation with a 5 ns laser pulse at 500 nm are shown in **Figure 5**a. The respective peak values of the photoconductance are used to calculate the product of the yield for free carrier generation per photon absorbed (φ) with the sum of the mobilities of electrons and holes ($\Sigma\mu$) as described in Equation 5 of the Experimental Section. The $\varphi\Sigma\mu$ product of pure P3HT, P3HT:PCBM and P3HT blended with ICMA, ICBA, and ICTA is shown versus absorbed photon flux of the incident excitation pulse (I_0F_A, see Equation 5) in Figure 5b. All samples exhibit a sublinear dependence of $\varphi\Sigma\mu$ on I_0F_A,[18] caused by exciton-carrier quenching processes at high excitation intensities.[9c,18c] The high $\varphi\Sigma\mu$ observed in the P3HT:PCBM sample compared to the pure P3HT film (Figure 5b) is attributed to the increase of the yield for free carrier generation, φ, when the acceptor is present and the contribution to $\Sigma\mu$ of the mobility of electrons in PCBM domains.[9c,18c] Pure P3HT is an excitonic semiconductor[19] with a low φ of ca. 2-6%,[9c,18] and in this case $\Sigma\mu$ is dominated by the high-frequency mobility of holes in the polymer, measured to be 0.014 cm^2 V^{-1} s^{-1} using pulse-radiolysis TRMC.[20] When PCBM is added to P3HT, φ increases by more than an order of magnitude,[9a,18c,21] and $\Sigma\mu$, in addition to the hole mobility, includes the mobility of electrons in the PCBM phase.[9] Recent reports estimate the electron mobility in P3HT:PCBM blends measured by TRMC to be between 0.03 and 0.06 cm^2 V^{-1} s^{-1},[9] i.e., higher than the hole mobility in P3HT, therefore the dominant contribution to $\Sigma\mu$ in these blends comes from the electron mobility in the fullerene domains.

The solid lines in Figure 5b are fits to the data using Equation 6 of the Experimental Section. From these we extract the low-intensity limit of $\varphi\Sigma\mu$, or, equivalently, the linear response limit of the photoconductance, in the absence of higher order loss mechanisms.[9c,22] The values are summarized in **Table 2**.

The values of $\varphi\Sigma\mu$ obtained for P3HT and for P3HT:PCBM (Table 2) are in good agreement with previous work,[9,18c] and can be used to estimate φ if $\Sigma\mu$ ($= \mu_e + \mu_h$) is known. For pure

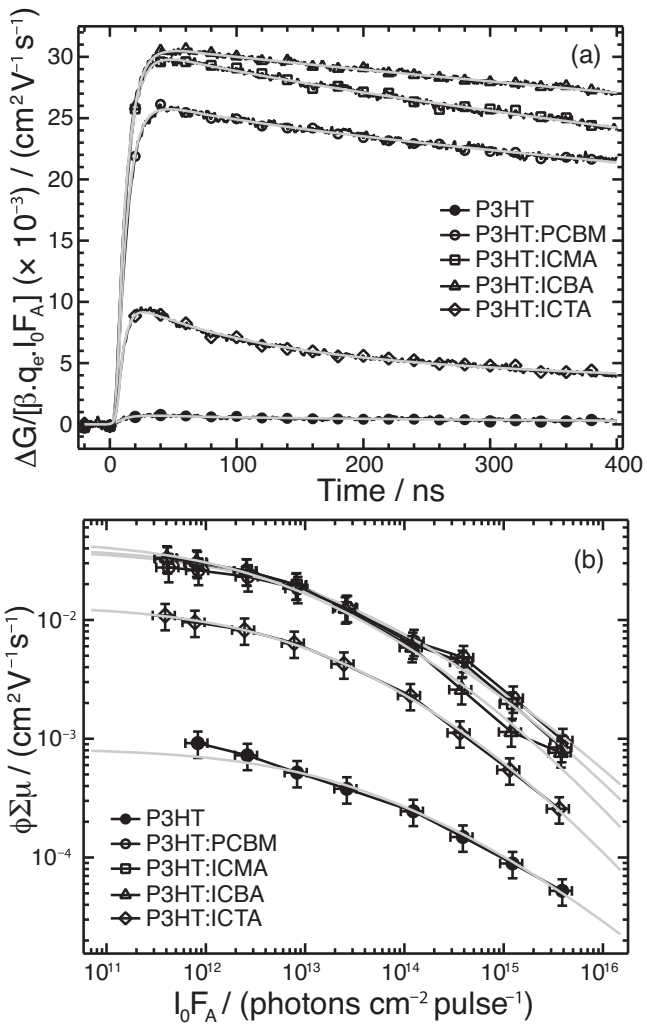

Figure 5. a) Photoconductance decay transient of P3HT and P3HT:fullerene films. Excitation was performed at a wavelength of 500 nm with a photon flux of ca. 8×10^{11} photons cm^{-2} $pulse^{-1}$. Solid lines are fits to the transient data using Equation 3. b) The end-of-pulse (EOP), or maximum, values of the $\varphi\Sigma\mu$ as a function of photon flux for P3HT and P3HT:fullerene films. Solid lines are fits to the data using Equation 6.

P3HT $\Sigma\mu = 0.014$ cm^2 V^{-1} s^{-1}[20] (i.e., the hole mobility) therefore one can estimate $\varphi = 6 \pm 3\%$, which is comparable to previous reports.[9c,18]

The magnitude of $\varphi\Sigma\mu$ for ICMA and ICBA blended with P3HT is very similar to that of P3HT:PCBM, indicating efficient charge carrier generation in these blends, as expected. As we will show in detail below, the yield for free carrier generation, φ, changes very little between these three donor-acceptor blends, and the subtle changes observed in $\varphi\Sigma\mu$ are primarily due to changes in the electron mobility contribution to $\Sigma\mu$. Assuming quantitative free carrier generation per photon absorbed ($\varphi = 100\%$) and only holes in the polymer are mobile, the $\varphi\Sigma\mu$ product gives a value of 0.014 cm^2 V^{-1} s^{-1}, which is ca. a factor 3 lower than $\varphi\Sigma\mu$ measured for P3HT with ICMA and ICBA. This indicates a significant contribution to $\Sigma\mu$ from the electron mobility in the fullerene domains for ICMA and ICBA, consistent with the observation of mobile electrons in the fullerene phase in photoexcited P3HT:PCBM blends.[9c] By contrast, $\varphi\Sigma\mu$ for P3HT:ICTA is very close to 0.014 cm^2 V^{-1} s^{-1}, which, as we will further discuss below, is indicative of only a small contribution to $\Sigma\mu$ from the electron mobility in this case.

We have recently developed a methodology to decouple the yield and mobility contributions from the $\varphi\Sigma\mu$ product determined by TRMC.[9c] We do so by using TCSPC to independently estimate the efficiency of exciton quenching in the blends, φ_b, given by:

$$\phi_b = 1 - \frac{\tau_b}{\tau_n}(1 - \phi_n) \quad (1)$$

where τ_b and τ_n, are the exciton lifetime in P3HT:fullerene blends and the intrinsic lifetime of the exciton in pure P3HT, respectively, and φ_n is the intrinsic quantum yield for free carrier generation in pure P3HT.[9c,18] For example, given an intrinsic yield for free carrier generation in pure P3HT φ_n = 6%, as estimated above, and the exciton lifetimes in P3HT (324 ps) and P3HT:PCBM (53 ps), we estimate that 85% of excitons are quenched in P3HT:PCBM, in agreement with previous reports.[9a,9c,21] While quenching of an exciton does not necessarily lead to an uncorrelated pair of free carriers, in the case where the internal quantum efficiencies obtained in a device are reasonably high (such as in P3HT:PCBM[7]) one can safely ignore loss pathways that do not lead to free carriers following exciton dissociation at the donor-acceptor interface,[6] and use the exciton dissociation efficiency estimated above as a good approximation to the yield for free carrier generation. Photoinduced absorption measurements in P3HT:PCBM have also suggested very efficient photoinduced generation of polarons.[6,21] In the following we will use the efficiency of exciton quenching obtained from TCSPC as an estimate of the yield for free carrier generation in blends of P3HT with all three indene-C_{60} acceptor derivatives. This is justified for the samples with ICMA and ICBA because they have a J_{sc} that is similar to the device with PCBM (Figure 4), suggesting no major loss pathways for exciton dissociation

Table 2. Photoconductivity and photoluminescence characterization for pristine P3HT and 1:1 P3HT:fullerene blends.

Sample	$\varphi\Sigma\mu$[a)] [$\times 10^{-2}$ cm^2 V^{-1} s^{-1}]	τ_{exc} [ps]	φ [%]	μ_e[d)] [$\times 10^{-2}$ cm^2 V^{-1} s^{-1}]
P3HT	0.08 ± 0.01	324 ± 46	6 ± 3[b)]	–
P3HT:PCBM	4.06 ± 0.78	53 ± 11	85 ± 28[c)]	3.38 ± 1.12
P3HT:ICMA	4.09 ± 0.95	64 ± 12	81 ± 26[c)]	3.65 ± 1.20
P3HT:ICBA	4.75 ± 0.84	62 ± 10	82 ± 27[c)]	4.39 ± 1.45
P3HT:ICTA	1.34 ± 0.28	95 ± 15	73 ± 24[c)]	0.44 ± 0.15

[a)] $\varphi\Sigma\mu$ is given by A in Equation 6 in the Experimental Section; [b)]Calculated from $\varphi\Sigma\mu$, under the assumption that the mobility product, $\Sigma\mu$, is determined by the high-frequency hole mobility in P3HT, μ_h = 0.014 cm^2 V^{-1} s^{-1};[20] [c)]Calculated using Equation 1 from the exciton lifetime in the P3HT:PCBM blend relative to that observed in neat P3HT (see main text for further details); [d)]Calculated from $\varphi\Sigma\mu$ and $\Sigma\mu = \mu_h + \mu_e$ under the assumption that the hole mobility in P3HT is μ_h = 0.014 cm^2 V^{-1} s^{-1}.[20]

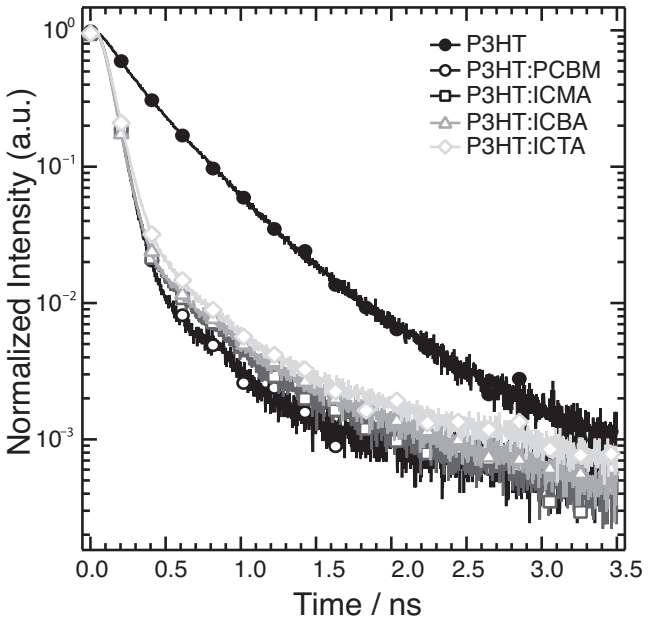

Figure 6. Semi-logarithmic plot of the PL decays of pristine P3HT and P3HT:fullerene films. The average lifetimes are 324, 53, 64, 62, and 95 ps, respectively, for P3HT (filled circles), P3HT:PCBM (circles), P3HT:ICMA (squares), P3HT:ICBA (triangles), and P3HT:ICTA (diamonds).

in the blend other than the generation of free carriers. While this reasoning cannot be used for the P3HT:ICTA sample, TRMC clearly shows enhanced free carrier generation with respect to the pristine polymer, hence we will use the same assumption and show that it leads to a self-consistent picture between the dynamics of free carrier generation as measured by TCSPC, the decay dynamics of the photoconductance as measured by TRMC, and the performance of photovoltaic devices.

Normalized TCSPC decays for P3HT, along with those for all the P3HT:fullerene blends, are shown in **Figure 6**. All were samples excited at 438 nm and their photoluminescence was detected at 720 nm. The decays for all samples can be accurately described using a bi-exponential decay, which means that the average exciton lifetimes can be obtained by:

$$\tau_{exc} = \frac{A_1\tau_1 + A_2\tau_2}{A_1 + A_2} \quad (2)$$

where A_i and τ_i are the amplitudes and the time constants for component *i*. The results are shown in Table 2. The average exciton lifetimes of P3HT (324 ps) and P3HT:PCBM (53 ps) are in good agreement with previous studies.[23] The exciton lifetimes in the P3HT:ICMA (64 ps) and P3HT:ICBA (62 ps) blends indicate efficient free carrier generation (ca. 80%) in these systems. The longer exciton lifetime measured in the P3HT:ICTA blend (95 ps) suggests a slightly lower efficiency of exciton quenching and free carrier generation (73%). We conclude that the lower driving force for exciton dissociation in the blends of P3HT with the indene-C_{60} derivatives, caused by the lower EA_A of the acceptors, does not limit the efficiency of exciton dissociation in these systems.

The estimates of the yield for free carrier generation allow us to decouple the yield-mobility product and calculate the high-frequency electron mobility in the acceptor domains, using the known high-frequency hole mobility in P3HT of 0.014 cm^2/Vs.[20] The values, listed in Table 2, show that the electron mobility in domains of ICMA and ICBA is of similar magnitude to that in PCBM, however it drops by a factor 10 in ICTA. We note that similar trends were found for the 'bulk' electron mobility measured for neat films of multiadducts of PCBM, using a field effect transistor geometry,[4g] and blends of P3HT with multiadducts of PCBM, using a thin film transistor geometry.[4f]

The calculated electron mobilities indicate that in blends of P3HT with ICMA and ICBA the electron term has a higher contribution to the photoconductance than the hole term (Equation 5) since the electron mobility is 2-3 times higher than the hole mobility (Table 2). By contrast, the electron mobility in the P3HT:ICTA is a factor of 3 lower than the hole mobility in P3HT, i.e., in this case the mobile holes dominate the photoconductance. The low J_{sc} of the P3HT:ICTA device (Figure 4 and Table 1) is therefore attributed to low electron mobility and not to low efficiency for free carrier generation.

2.5. Analysis of the Photoconductance Decay

Thus far we have only discussed the peak photoconductance as a measure of the yield for free carrier generation and their mobility. The normalized photoconductance decays of the samples used in this study, P3HT, P3HT:PCBM and P3HT blended with ICMA, ICBA and ICTA are shown in **Figure 7**. In order to extract the salient features of the decay for each sample we fit the transients with the following function:

$$\Delta G_{\exp}(t) = (\beta q_e d)\left(\sum \mu\right)\left[\frac{n_0 k}{(k + n_0\gamma)\, e^{kt} - n_0\gamma} + n_1 e^{-k_1 t}\right] \quad (3)$$

where *d* is the penetration depth of the excitation light into the sample (~100 nm for photoexcitation at 500 nm).[18b] Equation 3 is comparable to Equation 4 of the Experimental section, with the term in brackets being the time-dependent concentration of free carriers. The first term in the brackets is the analytical solution for a differential rate equation with competing first- and second-order decay processes,[18c] with rate constants *k* and γ, respectively. Whereas the second-order process corresponds to simple free carrier recombination, the first-order term is associated with the re-establishment of equilibrium between free and trapped carriers, as observed in the numerical analysis of photoconductance transients in P3HT:PCBM blends.[9c] An additional exponential term, characterized by the decay constant k_1, is also included to account for the long-lived carrier density observed in these systems.[18c] The initial carrier concentration, as generated by the laser pulse, is given by (n_0 + n_1). We use Equation 3, convoluted with a suitable instrument response function,[18c] to fit all the transients for each sample globally, using the nonlinear least-squares fitting procedure (Levenberg—Marquardt algorithm) of the built-in Global Fit package implemented by Igor Pro V6.22A: for each sample the rate constants *k* and γ, and the parameters of the instrument

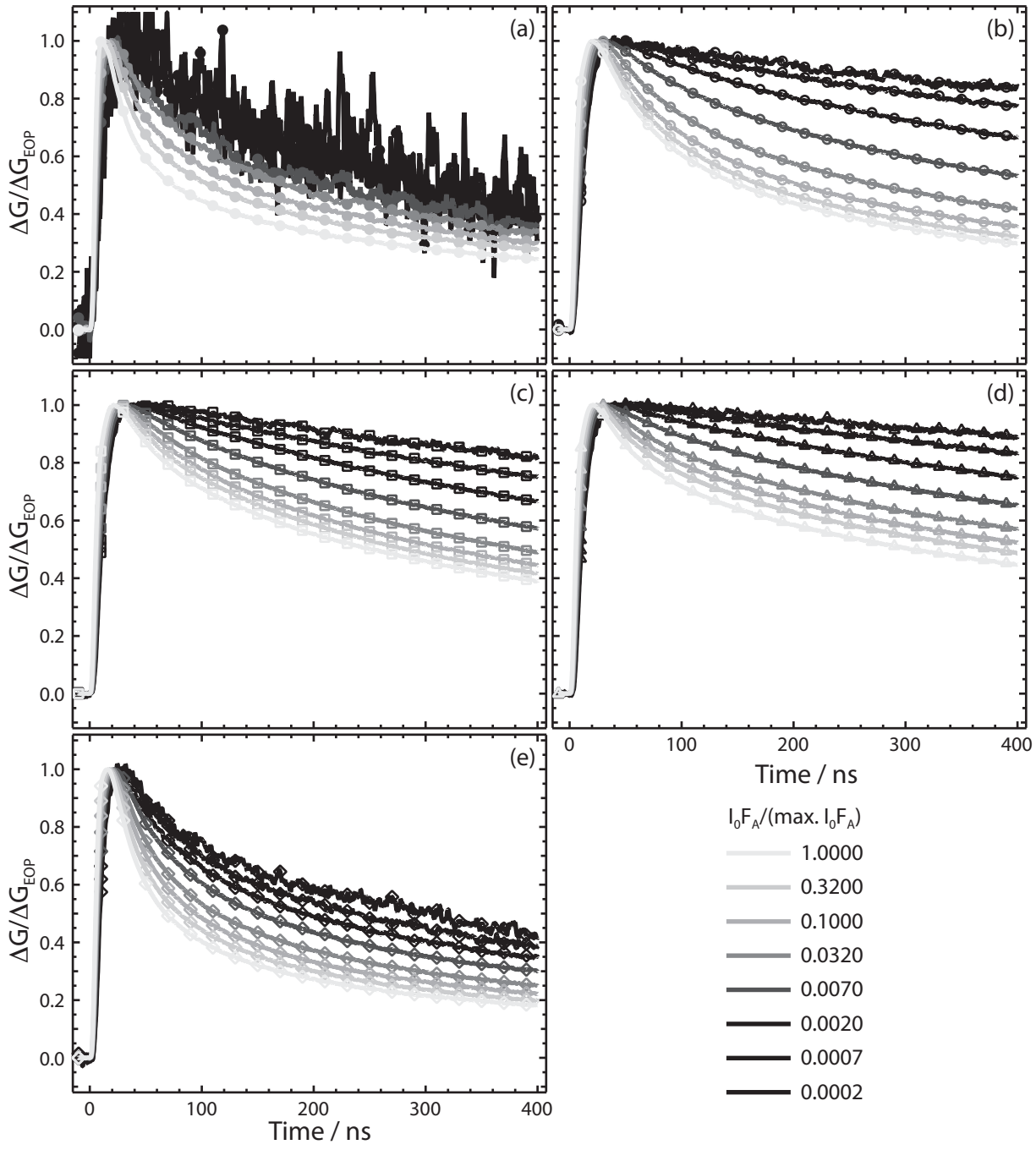

Figure 7. Photoconductance decays, normalized to the peak value, for a) pure P3HT, and blends of P3HT with b) PCBM, c) ICMA, d) ICBA, and e) ICTA. The traces presented span an excitation intensity range of ~8.2×10^{11} to ~3.8×10^{15} photons/cm^2/pulse, with the lighter traces representing the highest and the darker traces the lowest excitation intensities.

response function are "shared" for all excitation densities, while the initial concentrations, n_0 and n_1, and the rate constant of the long-time decay, k_1, are allowed to vary. The sum of the mobilities for each sample is fixed to the values estimated above (Table 2). Good fits to the transients for all samples were obtained with this procedure; representative fits are included in Figure 5a.

The fit parameters k, γ and k_1 for P3HT and the blends are listed in **Table 3**. The second-order rate coefficient, ascribed to recombination, γ, in P3HT:PCBM and in the blends of P3HT with ICMA and ICBA is lower by a factor of 6-7 compared to pure P3HT. A more rigorous numerical analysis of TRMC transients of P3HT and P3HT:PCBM, using a kinetic scheme to describe the evolution of photoinduced carriers gave a similar

Table 3. Rate coefficients extracted from photoconductance transient modeling for pristine P3HT and 1:1 P3HT:fullerene blends using Equation 5.

Sample	k [$\times 10^7$ s^{-1}]	γ [$\times 10^{-12}$ cm^3 s^{-1}]	k_1 [$\times 10^7$ s^{-1}]
P3HT	2.0 ± 0.4	70 ± 14	2.06–2.50
P3HT:PCBM	3.5 ± 0.6	11 ± 3	0.54–4.84
P3HT:ICMA	3.4 ± 0.8	10 ± 2	0.95–4.43
P3HT:ICBA	4.8 ± 1.0	9 ± 2	0.83–3.60
P3HT: ICTA	2.6 ± 0.6	50 ± 10	4.78–5.44

result for the recombination rate coefficient in pure P3HT and P3HT:PCBM.[9c] That analysis showed that in pristine P3HT recombination occurs between photoinduced holes and a large (>>10^{16} cm^{-3}) density of trapped electrons that is present in the dark and is minimally perturbed under illumination.[9c] Since in pristine P3HT the photoconductance is dominated by the contribution of free holes,[9a,9c,18,20] this mechanism results in a pseudo-first-order decay of the photoconductance transients of pure P3HT, in agreement with the weak intensity dependence of the transient profiles shown in Figure 7a. In contrast, the separation of carriers into different phases in P3HT:PCBM blend means that recombination of electrons in the fullerene phase occurs with free holes in P3HT via the interface between the two materials. This spatial separation of the carriers results in a reduced second-order rate coefficient γ,[9c] (Table 3). The existence of high-frequency electron mobility in the fullerene phase of the blends (in the case of PCBM, ICMA and ICBA) makes the electron term the dominant contribution to the photoconductance, resulting in strongly intensity-dependent decay profiles. Since the enhanced photoinduced free carrier yield in the blend produces free hole densities larger than the dark electron density in the pristine polymer the recombination process retains its second-order character. The strong light intensity dependence of the photoconductance decays for P3HT blended with ICMA and ICBA arise from the similarity of γ to that determined for P3HT:PCBM (Table 3), and the competition between the first- and second-order processes described by k and γ, respectively. In the P3HT:PCBM blend this intensity dependence arises from the photoconductance transient being dominated by the intensity-dependent electron dynamics in these blends.[9c] We note that the observation of very similar values for the second order rate constant, γ, between the blends with PCBM, ICMA and ICBA suggests that the second-order recombination process does not depend on the energy difference between the electron in the LUMO of the acceptor and the hole in HOMO of the polymer.

With regards to the P3HT:ICTA transients, the intensity-dependence is intermediate between the pristine polymer and the other P3HT:fullerene blends, which is consistent with a smaller contribution of the electrons to the photoconductance, due to the reduced high-frequency mobility in ICTA compared to the other fullerene derivatives. The reduced electron mobility means that the photoconductance decay dynamics in the P3HT:ICTA system are dominated by the holes in P3HT, which follow pseudo-first order decay. This is further substantiated by the magnitudes of k and γ, which are similar to the values observed for pristine P3HT.

The long-time (>100 ns) photoconductance decay dynamics are parametrized by k_1: the magnitude of the spread of k_1 values with varying light intensity gives an indication of the dispersive nature of the transients. Table 3 shows that in the case of both the pristine polymer and the P3HT:ICTA blend the spread in k_1 is small, indicating that the increased rate of recombination prevents carriers from sampling a large number of traps prior to annihilation. In contrast, the reduced recombination rate constant in the other P3HT:fullerene blends means that the carriers are longer-lived and can therefore sample a greater number of traps, thereby increasing the dispersive nature of the transients on a long timescale.

3. Conclusions

In addition to the expected presence of multiple regioisomers, resulting from the different possible patterns for the addition of substituents to a fullerene cage, chemical characterization of the indene-C_{60} multiadduct samples used in this study suggest that lower and/or higher adducts may also be present. The presence of different species (i.e., ICBA in the ICMA sample, etc.) is likely to arise from using flash chromatography to separate the reaction products of a large scale synthesis of multi-indene-C_{60} derivatives, as is commonly done for commercial-scale reactions in the interest in controlling materials cost. It is therefore of value to examine the properties of these commercial fullerene derivatives and evaluate their performance as acceptors in OPV. Indeed, we have found clear differences in the acceptor performance of the ICMA, ICBA and ICTA samples and we have been able to identify the process limiting the performance of OPV devices with ICTA, as summarized below.

We have shown that the attachment of solubilizing indene units, in place of the traditional phenyl-butyric acid methyl ester solubilizing group, to the fullerene cage is a viable approach to optimizing the energetics and performance of P3HT:fullerene devices in agreement with previous studies.[4i,4m] The addition of one (ICMA) or two (ICBA) indene substituents gives rise to a reduction of the electron affinity of the acceptor, resulting in a significant increase in the V_{oc} of devices incorporating these derivatives as the electron acceptor. The inclusion of a third indene unit (ICTA), however, adversely impacts all device parameters resulting in a poor PCE, although TCSPC and FP-TRMC measurements suggest that the reduced driving force for exciton dissociation, originating from the lower electron affinity of the acceptor, is not sufficient to account for the poor device performance. Additionally, analysis of the time-resolved photoconductivity data suggests that the *local* electron mobility in tris-indene-C_{60} domains is reduced compared to PCBM and the ICMA and ICBA adducts. These observations suggest that the poor performance of P3HT:ICTA devices is due to poor electron transport, both within and between ICTA domains. The possible presence of lower adducts (ICMA in the ICBA sample and ICBA in the ICTA sample) and the similar magnitude of spread in the distribution of LUMO energies for regioisomers of the bis- and tris-indene adducts, as calculated by DFT, suggest that electron trapping at fullerene sites with

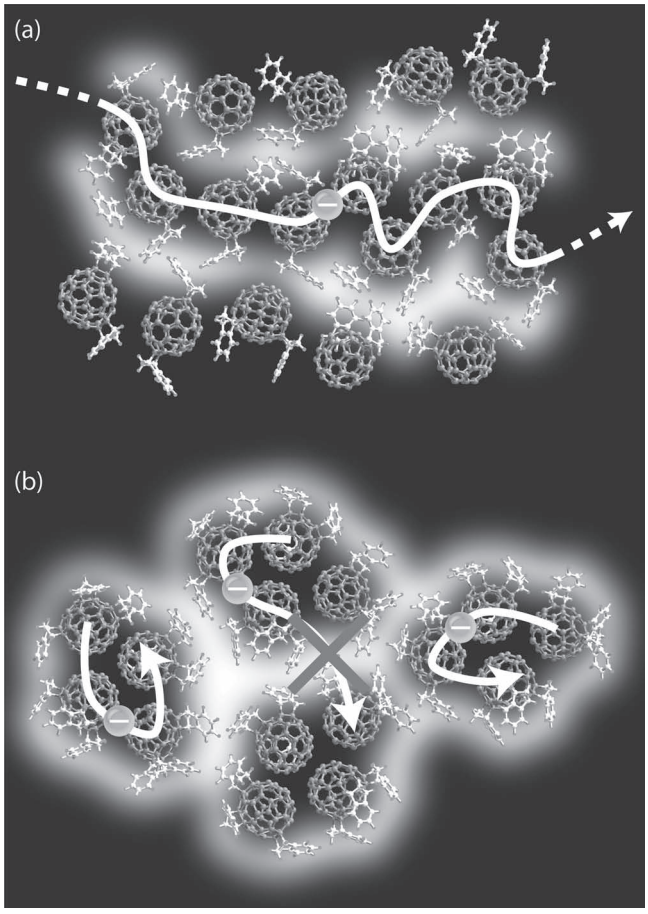

Figure 8. Cartoons showing the formation of two-dimensional clusters of a) ICBA and b) ICTA. In the case of ICBA the fullerene molecules are able to pack to form extended networks where the C_{60} cages are strongly coupled, facilitating high local and bulk electron mobilities. In contrast, small ICTA clusters can form where the electronic coupling between C_{60} cages is strong within the cluster but very weak between clusters, due to the insulating indene "coating." It should be noted that although the clusters will be three-dimensional the additional ICTA layers (omitted for clarity) will not form extended percolation networks.

low-lying LUMOs does not play a major role in device performance: if it did the devices with ICBA should also show poor electron mobility and poor performance, contrary to observations. We propose that the device performance is actually dictated by the ability of the indene-C_{60} multiadducts to pack effectively, and we demonstrate qualitatively that despite the regioisomerism present for ICBA the different isomers are still able to form extended structures where the electronic coupling between the fullerene cages is strong. In contrast, the addition of a third indene unit results in the formation of small clusters in which the fullerene cages are electronically coupled, but the insulating indene units are positioned on the outside of the cluster (**Figure 8**b) restricting both the local and bulk electron mobilities. The addition of the third indene substituent, and the concomitant increase in the number of possible tris-indene-C_{60} regioisomers, also results in significant structural disorder and hindered electron transport within the fullerene phase. Therefore, the disrupted "packing" of the fullerenes may also strongly influence the electronic coupling between neighboring fullerene molecules. Calculations of the electronic coupling between alkyl-substituted fullerene derivatives as a function of the alkyl chain length indicates that an increase in the separation between adjacent fullerene cages of only ~1 Å is sufficient to reduce the electron transfer integral by an order of magnitude.[10]

We conclude that despite the presence of multiple isomers, a fullerene sample may function well as an acceptor in OPV devices, as long as the fullerene cages can couple effectively to form percolation pathways for electrons. This implies that the laborious (and therefore expensive) separation of a fullerene sample into well-defined fractions (specific regioisomers etc.) may not be necessary for efficient devices. In agreement with previous studies of fullerene derivatives,[4f,4g,4m] these findings also suggest that there may be fundamental limitations to the extent to which multiadduct derivatization may be used as an approach to optimize the performance of OPV devices employing fullerenes an the electron-accepting component. That limitation primarily arises from the requirement for percolation through the fullerene phase.

4. Experimental Section

Materials and Film Fabrication: P3HT, mono- (ICMA), bis- (ICBA) and tris-indene-C_{60} (ICTA) were acquired from Plextronics Inc., whereas PCBM was purchased from Nano-C. The ICBA sample is the same as that used in the Plexcore PV2000 ink formulation and all indene-C_{60} derivatives have been purified according to the same standards. All materials were used as received.

Films for spectroscopic measurements and morphological characterization were deposited onto 10 × 24 mm quartz substrates that were prepared as described in the Supporting Information. Solutions of regioregular P3HT and P3HT:fullerenes (1:1 ratio by weight) in chloroform (CF) at a total active material concentration of 7.5 mg/mL. The solutions were stirred for at least 24 h at 40°C on a digitally controlled hot-plate in a N_2-filled glove box before being cooled to room temperature, filtered (at 0.45 μm), deposited onto the quartz substrates and allowed to slow dry in a covered petri-dish.

High-Performance Liquid Chromatography (HPLC): Indene-C_{60} samples from Plextronics, Inc. were used a received. HPLC grade toluene and heptane were used as received from Fisher Scientific. HPLC analyses were performed using a Shimadzu LC instrument (CBM-20A control module, SPD-20A UV detector, and LC-6AD pump) equipped with a Nacalai Tesque Cosmosil Buckyprep column (20 mm i.d. × 250 mm). A series of mobile phase eluent mixtures were tested to achieve optimal peak separation ranging from 100% toluene to 30/70 v/v toluene/heptane for each indene sample, and 10/90 toluene/heptane for tris-indene. Each sample solution was subjected to submicron filtration before analysis.

Cyclic Voltammetry: Cyclic voltammetry experiments were carried out in a nitrogen atmosphere glove box (water and oxygen content below 1 ppm) in a one-compartment electrochemical cell at room temperature. Solvent details are given in Supporting Information. The electrolyte solution was 0.1 M $N(n\text{-}Bu)_4BF_4$ in *o*-dichlorobenzene. Both $Fe(Cp^*)_2^{+/0}$ and $Fe(Cp)_2^{+/0}$ were used as internal standards, the scan speed was 20 mV s^{-1}, and a number of control experiments were conducted with C_{60} and the internal standards. From these control experiments, the error in the measurements to the 3 σ level was ± 0.01 V. The $E_{1/2}$ of $C_{60}^{0\backslash-}$ was measured to be -1.06 V vs. $Fe(Cp)_2^{+/0}$. The working electrode was a platinum wire (0.5 mm diameter). A platinum wire (0.5 mm diameter) and a silver wire (0.5 mm diameter) served as the counter electrode and quasi-reference electrode, respectively. The experiments were controlled by a PAR 263A potentiostat/galvanostat.

Density Functional Theory (DFT) Calculations: The LUMO energies of the different indene-C_{60} isomers were estimated to be those of the lowest unoccupied Kohn-Sham molecular orbitals computed with DFT for a geometry optimized for each isomer. Geometry optimization was performed using the Becke-style three-parameter density functional theory (DFT) method using the Lee-Yang-Parr correlation function (B3LYP) at the 6-31G(d) level and diffuse functions were included (6-31+G(d)) for calculation of the orbital energies of the optimized structures.

For the ICMA molecule, the indene moiety was placed so as to bridge a fullerene C = C bond shared by two hexagons (a [6,6] bond). It is well known that the formation of 4 + 2 cycloadducts of C_{60} invariably involve addition of the diene to a C_{60} [6,6] bond.[24] Furthermore, our DFT calculations show that the ICMA cycloadduct involving a [6,6] bond is more stable by ~81 kJ/mol than the ICMA cycloadduct involving a[5,6] bond at the B3LYP/6-31G(d) level of theory (this energy difference was essentially unchanged with the use of larger basis sets that included additional polarization functions, additional diffuse functions, or both). For these reasons, only cycloadditions involving [6,6] bonds were considered for the ICBA and ICTA isomers.

A set of isomers of ICBA and ICTA were generated considering all unique [6,6] bonds on the C_{60} cage, taking into account the relative orientations of the six-membered rings, as described in Supporting Information.

Device Fabrication and Measurement: OPV devices were prepared on patterned indium tin oxide (ITO) substrates that were cleaned as described in Supporting Information. Layers of poly(3,4-ethylene dioxythiophene):polystyrene sulfonate (PEDOT:PSS) (Baytron P VP AI 4083, filtered at 0.45 μm) of ~30 nm were spin coated on ITO and then annealed on a hotplate at 120°C, in air, for 1 h. The samples were then transferred to a glovebox for all remaining processing and characterization. Four blended solutions of P3HT and the fullerenes PCBM, ICMA, ICBA and ICTA were prepared (1:1 ratio by weight) with a total concentration of 50 mg/mL in dichlorobenzene (DCB). These were stirred on a hotplate at 60°C for at least 24 h prior to using and filtered with a 0.45 μm porous filter. The active layers were spun at 600 rpm for 60 s on top of the PEDOT:PSS layers, resulting in film thicknesses of around 250 nm. The samples were finally transferred to an evaporation chamber with a base pressure of 2×10^{-8} Torr for Al deposition (150 nm) at a rate of 2 Å/s. The complete devices were annealed at 150°C for 20 min before extracting their *J-V* characteristics (under AM1.5 conditions) with a Keithley 236 Source Measure Unit.

Flash-Photolysis Time-resolved Microwave Conductivity (FP-TRMC): Photocarrier dynamics were studied using FP-TRMC, a contactless, pump-probe technique where both the initial photogeneration of mobile carriers and their eventual decay back to equilibrium are monitored through the time-resolved changes in absorbed microwave power by the sample.[18a,18c,26] FP-TRMC measurements were performed at NREL using a system that has been described fully elsewhere.[18c,26b] The sample was placed in an X-band microwave cavity terminated with a grating reflective to microwaves but transparent to the optical excitation that was used to generate carriers within the film. All P3HT(:fullerene) films were excited through the quartz substrates with 5 ns laser pulses at 500 nm from an optical parametric oscillator (Continuum Panther) pumped by the 355 nm harmonic of a Q-switched Nd:YAG laser (Continuum Powerlite). The transient change in photoconductance, $\Delta G_{exp}(t)$, was measured via changes in the microwave power, $\Delta P(t)$, due to absorption of microwaves by the generated carriers, and is given by:

$$\Delta G_{exp}(t) = -\frac{1}{K}\frac{\Delta P(t)}{P} \tag{4}$$

where K is a calibration factor experimentally determined from the resonance characteristics of the microwave cavity and the dielectric properties of the sample.[18c,26b,27]

The end-of-pulse (peak) photoconductance, ΔG_{EOP}, can be related to the product of the yield for carrier generation, φ, and the sum of the high-frequency electron, μ_e, and hole, μ_h, mobilities in the blend, $\Sigma\mu$, by[18a]:

$$\Delta G_{EOP} = \beta q_e I_0 F_A \phi \sum \mu = \beta q_e I_0 F_A \phi (\mu_h + \mu_e) \tag{5}$$

where $\beta = 2.2$ is the ratio of the interior dimensions of the waveguide, q_e is the electronic charge, I_0 is the incident photon flux of the excitation pulse, and F_A is the fraction of absorbed photons.

At low absorbed photon flux ΔG_{EOP} increase linearly with I_0, however as the light intensity increases higher order processes become important, limit the carrier generation yield, φ, and the dependence becomes sublinear. The origin of the nonlinearity, originally attributed to rapid bimolecular recombination or exciton-exciton annihilation,[18a,18b] has more recently been proposed as exciton-hole quenching.[18c] We use Equation 6, which is a slight modification from a previous report,[18a] where it was used to describe data for neat P3HT, to extrapolate to the linear response limit of the photoconductance at low excitation intensities:

$$\frac{\Delta G_{EOP}}{\beta q_e} = \frac{A I_0 F_A}{1 + \sqrt{B I_0 F_A} + C I_0 F_A} \tag{6}$$

where A, B and C are fitting parameters. Comparison of Equation 5 and 6 allows us to obtain the low-intensity, linear response limit as $A = \beta q_e[\varphi\Sigma\mu]$.[9c,22]

Time-Correlated Single-Photon Counting (TCSPC): Photoluminescence (PL) decays were recorded, after excitation through the quartz substrate at 438 nm with a train of pulses (~150 ps FWHM), for emission at 720 nm, with a cooled photon counting photomultiplier tube (Hamamatsu H6279), using the TCSPC technique.[28] The PL decays were analyzed using an established non-linear least squares iterative reconvolution procedure,[29] where the finite width of the instrument response function was effectively deconvoluted from the measured data to give an overall temporal response of ~20 ps. Data were fit to a sum of two exponentials and the quality of fit judged using stringent statistical procedures.[28]

Supporting Information

Supporting Information is available from the Wiley Online Library or from the author.

Acknowledgements

The authors are grateful to Plextronics for providing materials for this work. This work was supported as part of the Energy Frontier Research Center "Molecularly Engineered Energy Materials (MEEMs)" funded by the U.S. Department of Energy, Office of Science, Office of Basic Energy Sciences under Contract Number DE-SC0001342:001. The chemical characterization of the indene-C_{60} adduct samples was carried out at Colorado State University: JBW, BWL, OVB, and SHS acknowledge the support of the U.S. National Science Foundation (CHE-1012468).

Received: February 3, 2012
Revised: April 19, 2012
Published online: June 11, 2012

[1] a) M. A. Green, K. Emery, Y. Hisikawa, W. Warta, *Prog. Photovolt. Res. Appl.* **2007**, *15*, 425; b) M. A. Green, K. Emery, Y. Hisikawa, W. Warta, E. D. Dunlop, *Prog. Photovolt. Res. Appl.* **2011**, *19*, 565.
[2] M. C. Scharber, D. Mühlbacher, M. Koppe, P. Denk, C. Waldauf, A. J. Heeger, C. L. Brabec, *Adv. Mater.* **2006**, *18*, 789.
[3] a) X. J. Wang, E. Perzon, J. L. Delgado, P. de la Cruz, F. L. Zhang, F. Langa, M. Andersson, O. Inganäs, *Appl. Phys. Lett.* **2004**, *85*, 5081; b) F. L. Zhang, E. Perzon, X. J. Wang, W. Mammo, M. R. Andersson, O. Inganäs, *Adv. Funct. Mater.* **2005**, *15*, 745;

c) D. Mühlbacher, M. Scharber, M. Morana, Z. Zhu, D. Waller, R. Gaudiana, C. Brabec, *Adv. Mater.* **2006**, *18*, 2884; d) M. Morana, H. Azimi, G. Dennler, H.-J. Egelhaaf, M. Scharber, K. Forberich, J. Hauch, R. Gaudiana, D. Waller, Z. Zhu, K. Hingerl, S. S. van Bavel, J. Loos, C. J. Brabec, *Adv. Funct. Mater.* **2010**, *20*, 1180; e) N. Blouin, A. Michaud, M. Leclerc, *Adv. Mater.* **2007**, *19*, 2295; f) Y. Liang, Y. Wu, D. Feng, S.-T. Tsai, H.-J. Son, G. Li, L. Yu, *J. Am. Chem. Soc.* **2009**, *131*, 56; g) H.-Y. Chen, J. Hou, S. Zhang, Y. Liang, G. Yang, Y. Yang, L. Yu, Y. Wu, G. Li, *Nat. Photonics* **2009**, *3*, 649.

[4] a) I. Riedel, N. Martin, F. Giacalone, J. L. Segura, D. Chirvase, J. Parisi, V. Dyakonov, *Thin Solid Films* **2004**, *451*, 43; b)I. Riedel, E. von Hauff, H. Parisi, N. Martin, F. Giacalone, V. Dyakonov, *Adv. Funct. Mater.* **2005**, *15*, 1979; c) S. A. Backer, K. Sivula, D. F. Kavulak, J. M. J. Frechet, *Chem. Mater.* **2007**, *19*, 2927; d) F. B. Kooistra, J. Knol, F. Kastenberg, L. M. Popescu, W. J. H. Verhees, J. M. Kroon, J. C. Hummelen, *Org. Lett.* **2007**, *9*, 551; e) M. Lenes, G.-J. A. H. Wetzelaer, F. B. Kooistra, S. C. Veenstra, J. C. Hummelen, P. W. M. Blom, *Adv. Mater.* **2008**, *20*, 2116; f) M. Lenes, S. W. Shelton, A. B. Sieval, D. F. Kronholm, J. C. Hummelen, P. W. M. Blom, *Adv. Funct. Mater.* **2009**, *19*, 3002; g) M. A. Faist, P. E. Keivanidis, S. Foster, P. H. Woebkenberg, T. D. Anthopoulos, D. D. C. Bradley, J. R. Durrant, J. Nelson, *J. Polym. Sci., Part B: Polym. Phys.* **2011**, *49*, 45; h) C. Yang, J. Y. Kim, S. Cho, J. K. Lee, A. J. Heeger, F. Wudl, *J. Am. Chem. Soc.* **2008**, *130*, 6444; i) Y. He, H.-Y. Chen, J. Hou, Y. Li, *J. Am. Chem. Soc.* **2010**, *132*, 1377; j) Y. He, H.-Y. Chen, G. Zhao, J. Hou, Y. Li, *Sol. Energy Mater. Sol. Cells* **2011**, *95*, 899; k) Y. He, H.-Y. Chen, G. Zhao, J. Hou, Y. Li, *Sol. Energy Mater. Sol. Cells* **2011**, *95*, 1762; l) R. B. Ross, C. M. Cardona, D. M. Guldi, S. G. Sankaranarayanan, M. O. Reese, N. Kopidakis, J. Peet, B. Walker, G. C. Bazan, E. Van Keuren, B. C. Holloway, M. Drees, *Nat. Mater.* **2009**, *8*, 208; m) H. Kang, C.-H. Cho, T. E. Kang, H. J. Kim, K.-H. Kim, H.-H. Cho, S. C. Yoon, B. J. Kim, *ACS Appl. Mater. Interfaces* **2011**, DOI: 10.1021/am201075y.

[5] J. M. Frost, M. A. Faist, J. Nelson, *Adv. Mater.* **2010**, *22*, 4881.

[6] H. Ohkita, S. Cook, Y. Astuti, W. Duffy, S. Tierney, W. Zhang, M. Heeney, I. McCulloch, J. Nelson, D. D. C. Bradley, J. R. Durrant, *J. Am. Chem. Soc.* **2008**, *130*, 3030.

[7] a) P. Schilinsky, C. Waldauf, C. J. Brabec, *Appl. Phys. Lett.* **2002**, *81*, 3885; b) J. Y. Kim, S. H. Kim, H. H. Lee, K. Lee, W. L. Ma, X. Gong, A. J. Heeger, *Adv. Mater.* **2006**, *18*, 572.

[8] D. W. Laird, R. Stegamat, H. Richter, V. Vejins, L. Scott, T. A. Lada, *Patent WO 2008/018931 A2*.

[9] a) W. J. Grzegorczyk, T. J. Savenije, T. E. Dykstra, J. Piris, J. M. Schins, L. D. A. Siebbeles, *J. Phys. Chem. C* **2010**, *114*, 5182; b) T. J. Savenije, D. H. K. Murthy, M. Gunz, J. Gorenflot, L. D. A. Siebbeles, V. Dyakonov, C. Deibel, *J. Phys. Chem. Lett.* **2011**, *2*, 1368; c) A. J. Ferguson, N. Kopidakis, S. E. Shaheen, G. Rumbles, *J. Phys. Chem. C* **2011**, *115*, 23134.

[10] R. C. I. MacKenzie, J. M. Frost, J. Nelson, *J. Chem. Phys.* **2010**, *132*, 064904.

[11] S. R. Cowan, W. L. Leong, N. Banerji, G. Dennler, A. J. Heeger, *Adv. Funct. Mater.* **2011**, *21*, 3083.

[12] A. Puplovskis, J. Kacens, O. Neilands, *Tetrahedron Lett.* **1997**, *38*, 285.

[13] H. Seyler, W. W. H. Wong, D. J. Jones, A. B. Holmes, *J. Org. Chem.* **2011**, *76*, 3551.

[14] Y. He, H.-Y. Chen, J. Hou, Y. Li, *J. Am. Chem. Soc.* **2010**, *132*, 5532.

[15] I. V. Kuvychko, A. V. Streletskii, N. B. Shustova, K. Seppelt, T. Drewello, A. A. Popov, S. H. Strauss, O. V. Boltalina, *J. Am. Chem. Soc.* **2010**, *132*, 6443.

[16] M. J. Frish, G. W. Trucks, H. B. Schlegel, G. E. Scuseria, M. A. Robb, J. R. Cheeseman, G. Scalmani, V. Barone, B. Mennucci, G. A. Petersson, H. Nakatsuji, M. Caricato, X. Li, H. P. Hratchian, A. F. Izmaylov, J. Bloino, G. Zheng, J. L. Sonnenberg, M. Hada, M. Ehara, K. Toyota, R. Fukuda, J. Hasegawa, M. Ishida, T. Nakajima, Y. Honda, O. Kitao, H. Nakai, T. Vreven, J. A. Montgomery Jr., J. E. Peralta, F. Ogliaro, M. Bearpark, J. J. Heyd, E. Brothers, K. N. Kudin, V. N. Staroverov, T. Keith, R. Kobayashi, J. Normand, K. Raghavachari, A. Rendell, J. C. Burant, S. S. Iyengar, J. Tomasi, M. Cossi, N. Rega, J. M. Millam, M. Klene, J. E. Knox, J. B. Cross, V. Bakken, C. Adamo, J. Jaramillo, R. Gomperts, R. E. Stratmann, O. Yazyev, A. J. Austin, R. Cammi, C. Pomelli, J. W. Ochterski, R. L. Martin, K. Morokuma, V. G. Zakrzewski, G. A. Voth, P. Salvador, J. J. Dannenberg, S. Dapprich, A. D. Daniels, O. Farkas, J. B. Foresman, J. V. Ortiz, J. Cioslowski, D. J. Fox, *Gaussian 09*, Revision B.01, Gaussian Inc., Wallingford CT, **2010**.

[17] C. J. Brabec, A. Cravino, D. Meissner, N. S. Sariciftci, T. Fromherz, M. T. Rispens, L. Sanchez, J. C. Hummelen, *Adv. Funct. Mater.* **2001**, *11*, 374.

[18] a) G. Dicker, M. P. de Haas, L. D. A. Siebbeles, J. M. Warman, *Phys. Rev. B* **2004**, *70*, 045203; b) G. Dicker, M. P. de Haas, L. D. A. Siebbeles, *Phys. Rev. B* **2005**, *71*, 155204; c) A. J. Ferguson, N. Kopidakis, S. E. Shaheen, G. Rumbles, *J. Phys. Chem. C* **2008**, *112*, 9865.

[19] B. A. Gregg, *J. Phys. Chem. B* **2003**, *107*, 4688.

[20] G. Dicker, M. P. de Haas, J. M. Warman, D. M. de Leeuw, L. D. A. Siebbeles, *J. Phys. Chem. B* **2004**, *108*, 17818.

[21] J. Piris, T. E. Dykstra, A. A. Bakulin, P. H. M. van Loosdrecht, W. Knulst, M. T. Trinh, J. M. Schins, L. D. A. Siebbeles, *J. Phys. Chem. C* **2009**, *113*, 14500.

[22] J. M. Holt, A. J. Ferguson, N. Kopidakis, B. A. Larsen, J. Bult, G. Rumbles, J. L. Blackburn, *Nano Lett.* **2010**, *10*, 4627.

[23] a) L. Magnani, G. Rumbles, I. D. W. Samuel, K. Murray, S. C. Moratti, A. B. Holmes, R. H. Friend, *Synth. Met.* **1997**, *84*, 899; b) P. E. Shaw, A. Ruseckas, I. D. W. Samuel, *Adv. Mater.* **2008**, *20*, 3516.

[24] A. Hirsch, M. Brettreich, *Fullerenes: Chemistry and Reactions*, Wiley-VCH Verlag GmbH & Co., Weinheim **2005**.

[25] A. Hirsch, I. Lamparth, H. R. Karfunkel, *Angew. Chem. Int. Ed.* **1994**, *33*, 437.

[26] a) J. E. Kroeze, T. J. Savenije, M. J. W. Vermeulen, J. M. Warman, *J. Phys. Chem. B* **2003**, *107*, 7696; b) J. Piris, N. Kopidakis, D. C. Olson, S. E. Shaheen, D. S. Ginley, G. Rumbles, *Adv. Funct. Mater.* **2007**, *17*, 3849.

[27] T. J. Savenije, M. P. de Haas, J. M. Warman, *Zeit. Phys. Chem.* **1999**, *212*, 201.

[28] D. Phillips, D. V. O'Connor, *Time-Correlated Single-Photon Counting*, Academic Press, London **1984**.

[29] A. Grinvald, I. Z. Steinberg, *Anal. Biochem.* **1974**, *59*, 583.